Simulation and Optimization of the Load Introduction Geometry of Additively Manufactured Lattice Structure Specimens

Sven Drücker[1], Stephan Inman[1] and Bodo Fiedler[1]

[1]Institute of Polymer Composites, Hamburg University of Technology, Denickestr. 15, 21073 Hamburg, Germany, Email: sven.druecker@tuhh.de, Web Page: http://www.tuhh.de/kvweb

Keywords: Lattice structure, Tensile test, Finite element method, Digital image correlation, Stereolithography

Abstract

Additively manufactured lattice structures show potential in medical and lightweight applications due to scalability of mechanical properties by the relative density of the cells. This requires characterization of the effective mechanical properties. Often compressive tests are used, however, tensile tests are conducted rarely despite their physical relevance. Current studies show challenges especially in determining reliable values of the effective tensile strength since specimens often fail at the transition from load introduction to lattice structure. The goal of this contribution is to provide guidelines for constructing load introduction geometries leading to failure of the samples within the lattice structure. To optimize the load introduction geometry, nonlinear finite element simulations are performed to identify stress concentrations. Tensile, compressive and single-edge-notch bending experiments of the stereolithography manufactured base material are conducted to calibrate the material model. The simulations show that confined transversal contraction is problematic and that a smooth transition with decreasing relative density of the lattice cells seems promising to determine reliable effective mechanical properties. To validate the simulations, tensile tests of lattice structure specimens with 3D digital image correlation are conducted.

1 Introduction

3D printing allows manufacturing of complex lattice structures. The application of these lattice structures are interesting for many different fields. They can be used as structured packings in process engineering [1] or as impact energy absorbers [2]. Another application is in the medical field as a replacement for bones that also show a porous structure [3]. Moreover, lattice structures show potential in lightweight applications [4]. Their mechanical properties can be scaled by the relative density and adapted to the local requirements given by the load paths. In order to use lattice structures as building blocks in topology optimization, a mechanical characterization is necessary. Compressive tests are often used in the literature to determine effective mechanical properties [5]. Also compressive cyclic loading has been analyzed [3]. However, tensile tests are conducted rarely despite their physical relevance. Current studies show challenges especially in determining the effective tensile strength. Specimens often fail at the

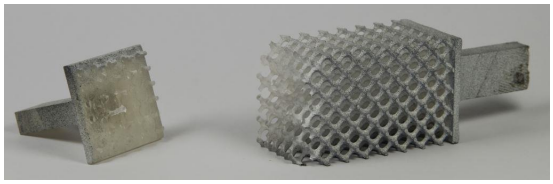

Figure 1: Tensile lattice specimen with failure near the load introduction.

transition from load introduction to lattice structure resulting in unreliable properties [6]. Figure 1 shows a tensile lattice specimen with failure near the load introduction.

The goal of the this contribution is to provide guidelines for constructing load introduction geometries that result in a homogeneous stress distribution within the cells, leading to failure of the samples within the lattice structure. To optimize the load introduction geometry, nonlinear finite element method (FEM) simulations are performed to identify stress concentrations. A parametric model for the geometry of the lattice structure specimens is generated with a PYTHON script in ABAQUS to be able to easily vary the load introduction. The material model is calibrated with the results of mechanical experiments of the base material for the stereolithography generated lattice structures. Tensile, compressive and single-edge-notch bending (SENB) tests are performed. To validate the simulations, the optimized specimens are printed in a stereolithography process. Tensile tests with 3D digital image correlation (DIC) are conducted to determine the effective mechanical properties.

2 Methods

In this section, the materials and sample preperation are described, the mechanical testing appraoch with usage of DIC measurements is presented and the FE model is explained.

2.1 Materials and Sample Preparation

The specimens are generated in the stereolithograpy process with the 3D printer FORMLABS Form 2. The photopolymer resin Clear provided by FORMLABS is used in the printer. For the mechanical characterization of the material, three experiments with different specimens are carried out. For tensile tests according to DIN EN ISO 527-2 [7] specimen type 1BB is used. The dimensions of the narrow parallel part of the specimen are $12\,\text{mm} \times 2\,\text{mm} \times 2\,\text{mm}$. Compressive tests are conducted according to DIN EN ISO 604 [8] with specimen type B. The dimensions of the rectangular block specimen are $10\,\text{mm} \times 10\,\text{mm} \times 4\,\text{mm}$. The critical strain energy release rate is determined with SENB specimens according to ASTM D5045 [9] with dimensions $40\,\text{mm} \times 8\,\text{mm} \times 4\,\text{mm}$. The specimens are constructed with the computer aided design (CAD) software AUTODESK INVENTOR and exported as standard tesselation language (STL) files for the printing process. Because of geometric simplicity, the specimens for the material characterization are printed with a layer height of $100\,\mu\text{m}$. The lattice structure specimens are constructed with the FEM software ABAQUS to have the geometry directly available and avoid import issues that arose during meshing. A PYTHON script is used, allowing for the automatic generation of parametric models. The analyzed lattice unit cells consist of three orthogonal struts with fillets to reduce stress concentrations. The initial specimens consist of cells with straight struts. The specimens with modified load introduction are composed of cells with struts having a gradually increasing diameter towards the load introduction to reduce jumps in stiffness from bulk material to lattice structure. The load introduction consists of a base plate connected to a clamping area. A fillet is used to have an equally distributed load over all cells. An eighth of the lattice specimen models is shown in Fig. 2.

(a) Initial specimen.

(b) Specimen with gradually increasing strut diameter towards the load introduction.

Figure 2: Models of the lattice structure specimens (only an eighth is shown due to symmetry).

For the printing process, the models are again exported as STL files. The geometrically more complex lattice specimens are printed with a layer height of 25 µm. After printing, the support structures are removed and the contact points are polished with sand paper. The edges are not further polished to have an as-build state as in the inside of the lattice structures where polishing is not possible. A 4 mm notch in the SENB specimens is created with a 150 µm diamond sawing blade followed by introducing the natural crack with a razor blade in a sawing motion. For DIC measurements, the lattice structures are coated with white aerosol paint. After drying a speckle pattern with black aeresol paint is applied.

2.2 Mechanical Testing

Uniaxial tensile tests according to DIN EN ISO 527-2 [7] are performed on a Zwick Z2.5 universal testing machine with a crosshead speed of $1\,\mathrm{mm\,min^{-1}}$. The strain is measured with a Zwick videoXtens extensometer. The test setup is shown in Fig. 3a. In addition, uniaxial compressive tests according to DIN EN ISO 604 [8] are carried out on a Zwick Z010 universal testing machine with a crosshead speed of $1\,\mathrm{mm\,min^{-1}}$. The crosshead displacement is used for strain measurements. To avoid bulging of the specimens due to friction during testing, polypropylen films are placed between the plungers and the specimens. Figure 3b demonstrates the compressive test setup. The SENB tests according to ASTM D5045 [9] are executed on a Zwick Z2.5 universal testing machine. The specimens are supported by rollers with a diameter of 6 mm and a spacing of 32 mm. A crosshead speed of $10\,\mathrm{mm\,min^{-1}}$ is used. The experimental setup is presented in Fig. 3c. After mechanical testing, the initial crack length is determined under an Olympus BX51 light microscope.

(a) Tensile test.

(b) Compressive test.

(c) SENB test.

Figure 3: Experiments for the mechanical characterization of the utilized base material for stereolithography.

Finally, tensile tests with the lattice structure specimens are performed on a Zwick Z010 universal testing machine with a crosshead speed of $1\,\mathrm{mm\,min^{-1}}$.

2.3 Digital Image Correlation

In order to measure the strain of the lattice structure specimens, 3D digital image correlation with the GOM Aramis 4M system is used. On the one hand, this allows to investigate the strain field, visualizing local strains in the individual struts of the lattice. On the other hand, the macroscopic effective strain of the lattice cells can be measured without the influence of the load introduction geometry. 3D measurements are preferable over 2D measurements [10] since also cell struts that are not on the front plane can be analyzed. The effective engineering strain is determined by continously tracking the distance change between two points on the lattice cells as displayed in Fig. 4.

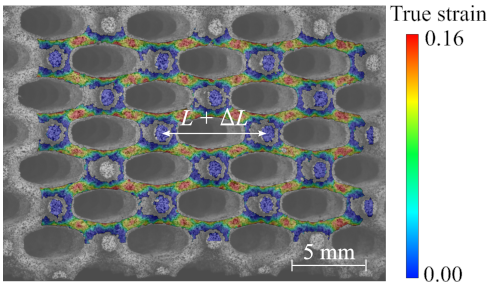

Figure 4: Measuring the effective engineering strain by tracking the distance change between two points in a DIC video.

2.4 Finite Element Model

FE simulations are performed with the commercial FE code ABAQUS 6.14. The boundary value problem of the dynamic equation of motion is solved with an implicit time integration method under consideration of finite deformations. The backward Euler operator is used which allows improved convergence behavior in case of instabilities because of progressive damage [11]. An unsymmetric equation solver is applied since symmetry of the material Jacobian is lost when ductile damage is utilized [11].

First, the tensile experiment is simulated to calibrate the material model. The simulation is displacement controlled. For the simulation of the tensile test, all three degrees of freedom are fixed at one side. At the other side, the transverse degrees of freedom are fixed and the displacement is applied in longitudinal direction. One element in the middle of the model has slightly reduced strength to initiate the localization of the plastic daformation.

Afterwards, the lattice structures with the load introduction are analyzed. The geometry of the lattice structures with the load introduction are constructed with a PYTHON script as described in Sect. 2.1. In order to save computational cost, only an eighth of the structure is modeled using symmetry in all three Cartesian coordinate directions. The deformation is displacement controlled at the end of the load introduction. The mesh is refined at the lattice structure and the transition to the load introduction and coarsened towards the clamping area of the load introduction. Thus, the interesting regions with stress concentrations can be analyzed with a high resolution and computational cost can be saved in unimportant regions. ABAQUS' C3D10 tetraheadral 3D continuum elements with quadratic shape functions are utilized for the discretization. These allow to resolve complex three-dimensional stress fields.

The material model is chosen according to the results of the mechanical characterization of the resin. An elastoplastic model with damage is applied. A built-in Drucker-Prager plasticity model is used to account for the tension-compression asymmetry in the yield stress. The general exponent form of the yield function Φ is given by

$$\Phi = a\sigma_{\mathrm{vM}}^{b} - p - p_t = 0\,, \tag{1}$$

where a and b are parameters independent of the plastic deformation, p_t is the hardening parameter representing the hydrostatic tensile strength and p is the hydrostatic pressure

$$p = -\frac{1}{3}\mathrm{tr}(\boldsymbol{\sigma})\,, \tag{2}$$

with $\mathrm{tr}(\boldsymbol{\sigma})$ being the trace of the Cauchy stress tensor. The von Mises equivalent stress σ_{vM} is given by

$$\sigma_{\mathrm{vM}} = \sqrt{\frac{3}{2}(\mathrm{dev}(\boldsymbol{\sigma}) : \mathrm{dev}(\boldsymbol{\sigma}))}\,, \tag{3}$$

with $\mathrm{dev}(\boldsymbol{\sigma})$ being the deviator of the Cauchy stress tensor

$$\mathrm{dev}(\boldsymbol{\sigma}) = \boldsymbol{\sigma} + p\mathbf{1}\,, \tag{4}$$

where $\mathbf{1}$ is the identity tensor. The hardening law is obtained by a multilinear curve from the uniaxial tension experiments.

For the damage initiation ABAQUS' built-in ductile criterion is used. Damage is initiated when the accumulated equivalent plastic strain $\bar{\varepsilon}_{\mathrm{p}}$ reaches the plastic strain at the onset of damage $\bar{\varepsilon}_{\mathrm{p,d}}$. After damage initiation, the stress carrying capability of the element is reduced linearly

$$\boldsymbol{\sigma}_{\mathrm{d}} = (1-d)\boldsymbol{\sigma}\,, \tag{5}$$

with $\boldsymbol{\sigma}_{\mathrm{d}}$ being the stress tensor of a damaged element and $d \in [0, 0.95]$ being the damage variable. To avoid mesh dependency, the damage evolution is implemented energy-based. The accumulated equivalent plastic strain at failure $\bar{\varepsilon}_{\mathrm{p,f}}$ is calculated with the critical energy release rate

$$G_{\mathrm{Ic}} = \int_{\bar{\varepsilon}_{\mathrm{p,d}}}^{\bar{\varepsilon}_{\mathrm{p,f}}} L\sigma_{\mathrm{y}}\mathrm{d}\bar{\varepsilon}_{\mathrm{p}}\,, \tag{6}$$

where L is the characteristic element length and σ_{y} is the yield stress. Viscous regularization is applied to overcome convergence difficulties [11].

3 Results and Discussion

In the following, the results of the material charaterization, the material model calibration and the lattice structures are presented and discussed.

3.1 Material Characterization

The results of the material characterization experiments for the FORMLABS clear resin are presented in Tab. 1 with number of repititions n, mean values and standard deviations (SD). The results are given in engineering stresses and strains. Especially, the significantly higher compressive yield stress compared to the tensile yield stress is noticeable. This requires to use an asymmetric tension-compression yield criterion in the simulations. As presented in Sect. 2.4 a Drucker-Prager yield surface is used to capture this. The presented results of the experiments are used in the following for the material model calibration.

Table 1: Results of the mechnical characterization of the FORMLABS clear resin.

Experiment	n	Parameter	Mean	SD
Tensile test	3	Modulus of elasticity E	1350.66 MPa	147.72 MPa
		Yield stress σ_y	29.65 MPa	0.71 MPa
		Elongation at break ε_b	17.06 %	6.40 %
Compressive test	5	Yield stress σ_y	61.55 MPa	1.32 MPa
SENB test	10	Critical energy release rate G_{Ic}	0.13 MPa mm	0.02 MPa mm

3.2 Material Model Calibration

As described in Sect. 2.4, the tensile test experiment is simulated to calibrate the material model since the hardening law is obtained from the uniaxial tension experiments. Figure 5 presents the boundary conditions of the model and shows a comparison of the experimental and simulated stress-strain curves. Good agreement is found in the specimen stiffness, the yielding regime, the decrease in engineering stress due to necking and the elongation at break.

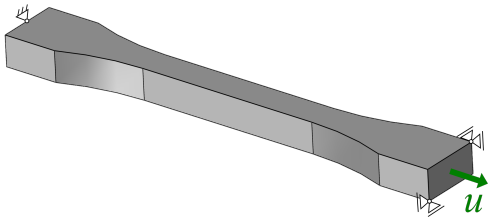

(a) Boundary conditions.

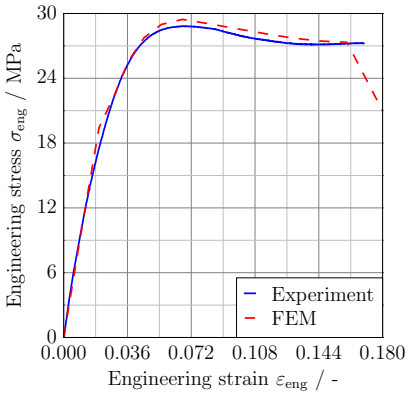

(b) Comparison of experiment an simulation.

Figure 5: Boundary conditions for the simulation of the tensile test and comparison of experimental and simulated engineering stress-strain curves.

3.3 Lattice Structures

The simulated damage locations of the lattice structure specimens are shown in Fig. 6a-6b with a contour plot of the damage variable. Due to the unit cell geometry and the ductility of the material, there is a strong transverse contraction. For the initial specimen, the transverse contraction is confined at the load introduction because of the much stiffer bulk material. Hence, the specimens fail at the transition from load introduction to lattice structure. For the modified geometry, the stiffness increases gradually towards the load introduction which results in failure inside the cells. In this case, fracture is also not in the same cell row over the whole cross-section but jumps through different rows. For the experimental characterization of the lattice structures, three specimens were tested. Figure 6c displays the failure location of the modified specimens in the experiments. Similar to the simulations, the modified specimens show the desired failure inside the lattice structure.

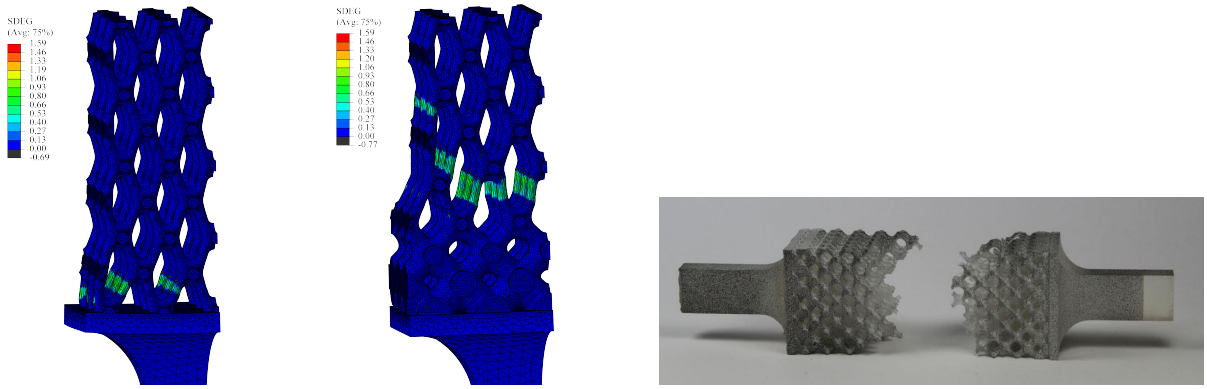

(a) Initial specimen. **(b)** Modified specimen. **(c)** Experimental failure within the lattice.

Figure 6: Damage locations for initial and modified lattice specimens where the strut diameter is increasing towards the load introduction.

4 Conclusion

A material characterization of the base material for the stereolithography process is carried out by tensile, compressive and SENB tests. The obtained properties are used in simulations. The tension-compression asymmetry is captured with a Drucker-Prager yield surface. A python script for the geometry generation of lattice structure and load introduction allows a systematic study of different load introductions. The simulations show that ductile material behavior and unit cell geometry lead to a strong transverse contraction. Confinement of the transverse contraction at the stiffer bulk material load introduction is the reason for failure of lattice structure specimens at the load introduction under tensile load. An increasing strut diameter towards the load introduction results in a smoother transition in stiffness from load introduction to lattice structure. Hence, fracture is shifted to the inside of the lattice structure. Tensile test experiments on modified lattice structure specimens validate the improved failure behavior.

Acknowledgement

Financial support from the Federal Ministry for Economic Affairs and Energy of Germany (BMWi) in the project “ALM2AIR” (project number: 20W1501M) is gratefully acknowledged. The authors thank Helge Hoch (Institute of Laser and System Technologies/Hamburg University of Technology) as well as Bich Ngoc Vu, Thomas Guess and Fabian Wein (Applied Mathematics 2/University of Erlangen-Nuremberg) for the collaboration within the project.

References

[1] A. Olenberg, W. Reschetnik, G. Kullmer, and E. Y. Kenig. “Optimization of structured packings using twisted tape inserts”. In: *Chemical Engineering Research and Design* 132 (2018), pp. 1 –8.

[2] G. W. Kooistra, V. S. Deshpande, and H. N. Wadley. “Compressive behavior of age hardenable tetrahedral lattice truss structures made from aluminium”. In: *Acta Materialia* 52.14 (2004), pp. 4229 –4237.

[3] S. Arabnejad Khanoki and D. Pasini. “Fatigue design of a mechanically biocompatible lattice for a proof-of-concept femoral stem”. In: *Journal of the Mechanical Behavior of Biomedical Materials* 22 (2013), pp. 65 –83.

[4] S. Merkt. “Qualifizierung von generativ gefertigten Gitterstrukturen für maßgeschneiderte Bauteilfunktionen”. Dissertation. Chair for Laser Technology/RWTH Aachen University, 2015.

[5] R. Gümrük and R. Mines. “Compressive behaviour of stainless steel micro-lattice structures”. In: *International Journal of Mechanical Sciences* 68 (2013), pp. 125 –139.

[6] H. Alsalla, L. Hao, and C. Smith. “Fracture toughness and tensile strength of 316L stainless steel cellular lattice structures manufactured using the selective laser melting technique”. In: *Materials Science and Engineering: A* 669 (2016), pp. 1 –6.

[7] German Institute for Standardisation. *Plastics - Determination of tensile properties - Part 2: Test conditions for moulding and extrusion plastics (ISO 527-2:2012)*. German Institute for Standardisation, 2012.

[8] German Institute for Standardisation. *Plastics - Determination of compressive properties (ISO 604:2002)*. German Institute for Standardisation, 2003.

[9] ASTM International. *ASTM D5045 - 14: Standard Test Methods for Plane-Strain Fracture Toughness and Strain Energy Release Rate of Plastic Materials*. ASTM International, 2014.

[10] B. Gorny, T. Niendorf, J. Lackmann, M. Thoene, T. Troester, and H. Maier. “In situ characterization of the deformation and failure behavior of non-stochastic porous structures processed by selective laser melting”. In: *Materials Science and Engineering: A* 528.27 (2011), pp. 7962 –7967.

[11] Dassault Systèmes. *Abaqus 6.14 Analysis User’s Guide*. Documentation. Dassault Systèmes Simulia Corp., 2014.